THE STUDIES OF SPECTRAL SPR MULTILAYERS DETECTOR RESPONSE BASED ON T-MATRIX INTENDED FOR BIOMEDICAL APPLICATION

Abdelali SAOULI[1], Chouaib SAOULI[2]

The SPR (Plasma Resonance Surface) detector in the biological field is based on noble metals, when the TM (transverse magnetic) wave with visible range arriving at the dielectric / metal interface and at the base of the reflection or transmission of this signal, can we ensure the creation of the SPR effect. However, the biological environments to be detected have an influence on the SPR effect, perhaps on the wavelength or the angle of incidence of the resonance. Thus, the SPR effect in the proposed multilayer nanostructures is modeled by the transfer matrix method (T matrix). Therefore, these structures can be used for detection in the biomedical field

Keywords: SPR effect, multi layers nanostructures, T-matrix.

1. Introduction

The application of SPR-based sensors to bio-molecular interaction monitoring-was first demonstrated in 1983 by Liedberget al [1]. The effect of the surface plasmon (SPR) present in several domains in force during the last years, in the detection of the DNA [2,3], the waveguides for application in biosensor [4,5], thus the detection of the bio corps [6]. Also, in biomedicine [7,8], bio analysis [9,10], optics [7,11] and solar energy [12]. Each application signifies by a specific structure, either metallic nanostructures continued [4,11] or discrete, for the latter finds spherical matrices [7,12], cylindrical [7], cubic [7], at the level of our work we are interested in the continuous structures based on thin metallic layers full. Indeed, the scientific researches in this new rich field are very active so that it integrates in the industry. For example, in the biomedical field, there are several marketed instruments that operate on the basis of the SPR effect such as Biacore X, 3000, S51 and X100 of GE Healthcare company, Reichert SR7500DC and 4SPR of Reichert Technologies company, BI-SPR of Biosensing Instruments company, SensiQ of SensiQ Technologies company, Open SPR of Nicoya instrument company, Indicator-G research platform of Sensia company, BioNavis MP-SPR Navit family of products: MPSPR Navit200 OTSO, MP-SPR Navit210A VASA, MP-SPR Navit220ANAALI, and MP-SPR Navit420A ILVES of BioNavis company, BIOSUPLAR-6 of Analyticalm-Systems company [13].

[1] Department of electronics, Mentouri Brothers University of Constantine. Constantine, Algeria, e-mail: abdelali.saouli@lec-umc.org

[2] Department of chemistry, Mentouri Brothers University of Constantine. Constantine, Algeria

The SPR effect is greater in noble metals whose imaginary part ε_2 of the dielectric function ($\varepsilon = \varepsilon_1 + i \times \varepsilon_2$) is weak. An important consequence of this is that a TE polarized light beam will not cause an oscillation of the charges at the metal /dielectric interface. There will be no excitation of surface plasmons for this polarization. On the contrary, an evanescent TM wave arriving at the dielectric/metal interface will decompose in this latter medium into a transverse wave and another longitudinal one. This longitudinal component of the wave in the metal will then create a longitudinal vector potential which will be able to couple to the oscillations of density of surface charges or surface plasmons [14]. Under proper conditions the reflectivity of a thin metal film is extremely sensitive to optical variations in the medium on one side of it, this is due to the fact that surface plasmons are sensitive probes of the boundary conditions [1]. The SPR detection technique based on two methods of detection, the angular interrogation (θ) which consists in supporting the angular position of the minimum reflectivity SPR at a wave length of incidence (λ) fixes, and the spectral interrogation that consists in supporting the spectral position (λ) of the minimum reflectivity SPR at an angle of incidence θ fixed. The study of spectral response of the multi layers SPR detector is based on the method of transfer matrices (T -matrix).

The rest of this paper is organized as follows. In Section II, present the Physic-mathematical system presentation. The proposed method is applied to modeling the plasmonic nanostructures response. Section III shows the numerical result and discussion. Section IV summarizes the contributions of this paper.

2. Physic-mathematical system presentation.

The structures to be studied in this work are based on multiple layers (Figure.1); this is the reason for our choice of the transfer matrix method (T matrix) in the simulation of the SPR response.

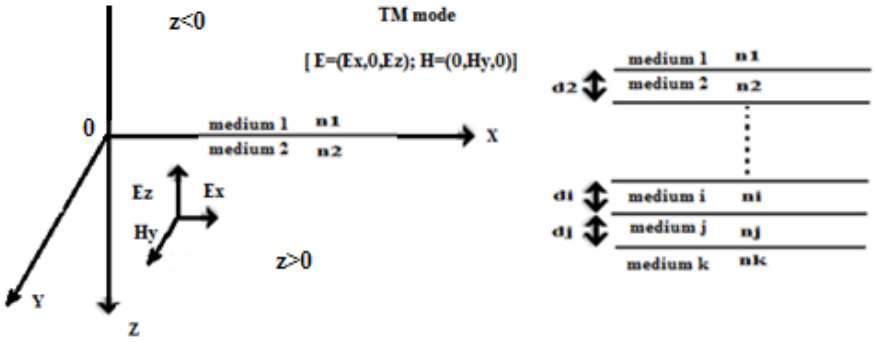

Fig 1. The model used in the matrix method for a multi-beam interface. The electric field moves from top (medium 1) to bottom (medium k) through mediums characterized by their refractive index ni and thickness di (the axis Z is the direction of propagation) [15].

Indeed, the surface plasmon wave is considered as an electromagnetic wave propagating along the metallic and dielectric interface. Subsequently, to explain the presence of surface plasmons, the analysis of the electromagnetic properties of the interfaces is necessary. This is why, in such an analysis, a key element is the dispersion relation, which describes the relation between the wave vector k and the angular frequency ω, and this will be derived in the following. In this study we have worked with electromagnetic fields (EM-fields) the central concept is electric wave equation derived from Maxwell equation [16]:

$$\nabla^2\vec{E} - \frac{\epsilon}{c^2}\frac{\delta^2\vec{E}}{\delta t^2} = 0 \tag{1}$$

Where ϵ is constant on the scale of one wavelength. It assumed that all electromagnetic waves solving this equation this equation have harmonic time dependence [16]:

$$\vec{E}(\vec{r},t) = \vec{E}(r)e^{-i\omega t} \tag{2}$$

Using this in equation 1, the time derivation can be solved, and thus the equation is reduced to:

$$\nabla^2\vec{E} - k_0^2\vec{E} = 0 \tag{3}$$

Where k_0 the propagation vector in vacuum (ω/c). A simple idealized set-up could be described as two partially infinite mediums (1 and 2) where medium one is characterized by a dielectric constant ε_1 and the other medium is a dielectric with dielectric constant ε_2. The two mediums are arranged so that the interface between the two is in the x, y plane (Figure 1). This means that dielectric constant only is function of z. Furthermore, the geometry is arranged so that the $\vec{E}$ field propagation along x axis, orthogonal to the y axis, making this two dimensional problem. This gives us possibility to write the E field as:

$$\vec{E}(x,y,z) = \vec{E}(z)e^{ik_x x} \tag{4}$$

Here, k_x is the propagation vector in the x direction. This used to further simplify the wave equation, by reducing the Laplace operator to second derivative in z direction:

$$\frac{\delta^2\vec{E}(z)}{\delta z^2} + (k_0^2 - \beta^2)\vec{E}(z) = 0 \tag{5}$$

As the electric field and the magnetic fields are coupled, a similar wave equation exists for the magnetic field, though it is not displayed here.

The investigator in this area notes that a more in-depth differential analysis will show that only the transverse magnetic or polarized p (TM) mode gives non-zero results [14], when the determination of eigenstates is governed by the following two equations, which are derived of the loop equations of maxwell's equations given by [16]:

$$E_x = -i\frac{1}{\omega\varepsilon_0\varepsilon}\frac{\delta H_y}{\delta z} \tag{6}$$

$$\mathrm{E_z} = -\frac{k_x}{\omega\varepsilon_0\varepsilon}H_y \tag{7}$$

And the wave equation for the y component of the H field given by [16]:

$$\frac{\delta^2 H_y}{\delta z^2} + (k_0^2 \varepsilon - k_x^2) H_y = 0 \quad (8)$$

Here, ε: Relative permittivity, ε_0: The electrical permittivity of the vacuum, ω:angular velocity of wave.

From this point, the resolution of this equation provides the following formula for $H_y(z)$ [15]:

$$H_y(z) = \begin{cases} Ae^{ik_x x} e^{k_{z,1} z}, for\ z < 0 \\ Ae^{ik_x x} e^{-k_{z,1} z}, for\ z > 0 \end{cases} \quad (9)$$

So, using this formula in equations 6 and 7 gives the equation that describes the E field at the interface (equation 10 and 11).

$$E_x(z) = \begin{cases} -iA \frac{1}{\omega \varepsilon_0 \varepsilon_1} k_{z,1} e^{ik_x x} e^{k_{z,1} z}, for\ z < 0 \\ iA \frac{1}{\omega \varepsilon_0 \varepsilon_2} k_{z,2} e^{ik_x x} e^{-k_{z,2} z}, for\ z > 0 \end{cases} \quad (10)$$

$$E_z(z) = \begin{cases} -A \frac{k_x}{\omega \varepsilon_0 \varepsilon_1} e^{ik_x x} e^{k_{z,1} z}, for\ z < 0 \\ -A \frac{k_x}{\omega \varepsilon_0 \varepsilon_2} e^{ik_x x} e^{-k_{z,2} z}, for\ z > 0 \end{cases} \quad (11)$$

Concerning boundary conditions at the interface (z=0), it's require continuity in the magnitude of the field H_y as well as in $\varepsilon_1 E_z$ and the values of the constants 'A' have the same value. This continuity also imposes the relation between the dielectric constants:

$$\frac{k_{z,2}}{k_{z,1}} = -\frac{\varepsilon_2}{\varepsilon_1} \quad (12)$$

This is one of the two relationships needed to obtain a dispersion relationship for surface plasmon waves. The other relation is obtained by entering the equation of H_y (equation 9 in the wave equation (equation 8)).

$$k_1^2 = k_x^2 - k_0 \varepsilon_1 \quad (13)$$

$$k_2^2 = k_x^2 - k_0 \varepsilon_2 \quad (14)$$

In the latter we conclude that the combination of these last three equations and the definition of the vacuum propagation vector $k_0 = \omega/c$ give us the dispersion relation:

$$k_x = \frac{\omega}{c} \sqrt{\frac{\varepsilon_1 \varepsilon_2}{\varepsilon_1 + \varepsilon_2}} \quad (15)$$

However, it can be deduced that the angular frequency depends on the dielectric constant, and therefore the refractive index, as $\varepsilon = n^2$. This derivation is however fairly basic, because it is only valid for an interface with metal and dielectric.

The SPR sensor used in the configuration is made up of several layers (Figure 2). There is therefore a more complex method which is therefore necessary to correctly

describe the expected signal. Thus, in order to obtain a theoretical model of the SPR profile, a matrix is used for multi-beam interference. For clarification, the following derivation is based on the work of Klein and Furtak [15]:

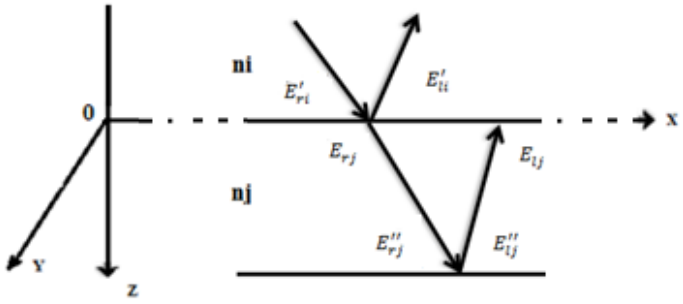

Fig.2. Detailed model of the optical situation analysed. The electric field (E'_{ri}) moves from top to bottom through the mediums characterized by their refractive indices ni and nj [15].

We have the transition of the fields at the interface between the medium i and j and given by [17]:

$$\begin{pmatrix} E'_{li} \\ E'_{ri} \end{pmatrix} = \frac{1}{\tau_{ij}} \begin{pmatrix} 1 & \rho_{ij} \\ \rho_{ij} & 1 \end{pmatrix} \begin{pmatrix} E_{lj} \\ E_{rj} \end{pmatrix} \tag{16}$$

and:

$$E' = H_{ij} E \tag{17}$$

Where H_{ij} is the matrix describing the transition of the fields on the interface between the media i and j and given by:

$$\mathrm{H_{ij}} = \frac{1}{\tau_{ij}} \begin{pmatrix} 1 & \rho_{ij} \\ \rho_{ij} & 1 \end{pmatrix} \tag{18}$$

Also, if the incident wave is polarized p (TM mode), so that the field E is in the plane incidence,τ_{ij} and ρ_{ji} are given by[15]:

$$\tau_{ij} = \frac{2(\tilde{n}_i/\tilde{n}_j)}{1+b} \tag{19}$$

And :

$$\rho_{ji} = \frac{1-b}{1+b} \tag{20}$$

Where:

$$b = \left(\frac{\tilde{n}_i}{\tilde{n}_j}\right)^2 \left(\frac{k_{z,j}}{k_{z,i}}\right) \tag{21}$$

Where, $\tilde{n}_i$ and $\tilde{n}_j$ is the complex reactivity index of the medium i and j, and $k_{z,j}$ is the reciprocal wave number of the field E in the medium j.

As well, the transition of the fields through the medium j and given by [17]:

$$\begin{pmatrix} E_{lj} \\ E_{rj} \end{pmatrix} = \begin{pmatrix} e^{\beta_j} & 0 \\ 0 & e^{-\beta_j} \end{pmatrix} \begin{pmatrix} E''_{lj} \\ E''_{rj} \end{pmatrix} = E \tag{22}$$

And:

$$E = L_j E'' = L_j \begin{pmatrix} E''_{lj} \\ E''_{rj} \end{pmatrix} \tag{23}$$

Where L_{ij} is the matrix for the transaction through the medium j using a phase factor e^{β_j} given by:

$$\mathrm{L_j} = \begin{pmatrix} \mathrm{e}^{\beta_j} & 0 \\ 0 & \mathrm{e}^{-\beta_j} \end{pmatrix} \tag{24}$$

Where β_j is given by [17]:

$$\beta_j = \frac{2\pi}{\lambda} n_j d_i cos(\theta_j) \tag{25}$$

Subsequently and by combining the matrices H and L of several layers, we obtain a total matrix, a complete stack of layers.

$$H_{12}L_2H_{23}L_3 \ldots H_{ij}L_j \ldots H_{N-1,N}L_N = S_{1N} = \begin{pmatrix} S_{11} & S_{12} \\ S_{21} & S_{22} \end{pmatrix} \tag{26}$$

Finally, the reflectance of the stack is then given by [15]:

$$R = \left|\frac{S_{21}}{S_{11}}\right|^2 \tag{27}$$

In our study, we based on the model of Drude with two critical points (D2CP) whose the metal dielectric function presented by the equation (28) [18].

$$\varepsilon_{D2CP} = \varepsilon_\infty + \frac{\omega_p^2}{\omega^2 + i\gamma\omega} + \sum_{i=1}^{2} A_i \Omega_i \left(\frac{e^{i\varphi_i}}{\Omega_i - \omega - i\Gamma_i} + \frac{e^{-i\varphi_i}}{\Omega_i + \omega + i\Gamma_i} \right) \tag{28}$$

The parameters of the D2CP model for gold and silver obtained in the 400-1000 nm optical range utilised in this study are presented in Table 1, this parameters optimized by A. Vial and T. Laroche [18].

Table 1

Optimized Parameters of the D2CP Model for Gold and Silver Obtained in the 400-1000 nm Optical Range [18].

	ε_∞	ω_p (rad.s^{-1})	γ (rad.s^{-1})	A_1	Ω_1 (RAD.S^{-1})	φ_1 (rad)	Γ_1 (rad.s^{-1})
Au	1.0300	1.3064×10^{16}	1.1274×10^{14}	0.86822	4.0812×10^{15}	-0.60756	7.3277×10^{14}
Ag	3.7325	1.3354×10^{16}	9.6875×10^{13}	2.0297	4.5932×10^{17}	-0.70952	1.0524×10^{18}
Al	1.000	2.0598×10^{16}	2.2876×10^{14}	5.2306	2.2694×10^{15}	−0.51202	3.2867×10^{14}
	A_2	**Ω_2 (rad.s^{-1})**	**φ_2 (rad)**	**Γ_2 (rad.s^{-1})**			
Au	1.3700	6.4269×10^{15}	-0.087341	6.7371×10^{14}			
Ag	-2.8925	4.7711×10^{16}	-1.4459	3.0719×10^{154}			
Al	5.2704	2.4668×10^{15}	0.42503	1.7731×10^{15}			

3. Results and discussion

The basic SPR detector based on three layers (Figure 3), metal with complex refractive indexes nm and two layers of dielectrics medium, one at the above with refractive indexes n1 and other the bottom with refractive indexes n2.

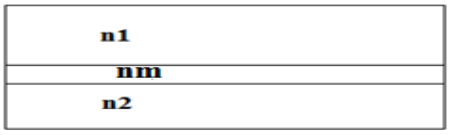

Fig 3. Structure of SPR-detector based on three layers.

The first studied based on three metals: Gold, Silver and Aluminum. The curves of reflectance versus wavelength and different thickness values of metal (Gold, Silver and Aluminum) are presented in Figs. 4, 5 and 6 respectively. Note that the SPR effect is present in all reflectance curves with the parametric and geometric conditions presented in the figures (Figs. 4.a, 5.a and 6.a). Also for the minimum reflectance (SPR) (Figs. 4.b, 5.b and 6.b), it is noted that it inscribes minimum values for thicknesses around 50 [nm] for the Gold (2% of reflectance), 40 [nm] for Silver (3 % of reflectance) and 15 [nm] for Aluminum (45% of reflectance). So, we can say that for a better resolution of the SPR effect and for the data of the simulation used, the ideal thickness is 50 [nm] for the Gold, 40 [nm] for Silver and 15 [nm] for Aluminum.

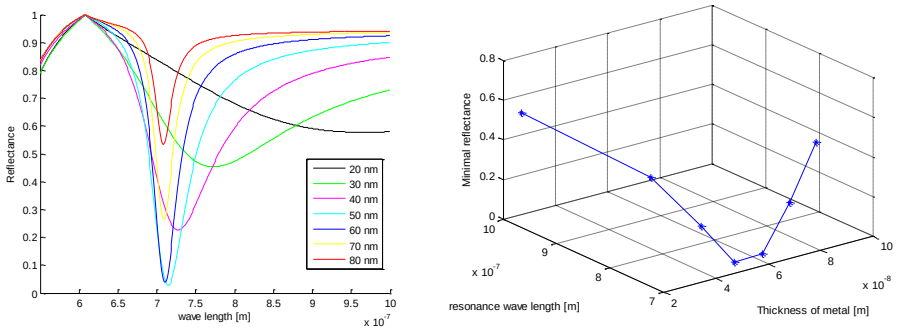

(a) *(b)*

Fig 4. a) Variation of the reflectance as a function of the wavelength and different values of dAu; b) Variation of the minimum reflectance as a function of the resonance wavelength and the metal thickness dAu: n1 = 2.39, n2 = 1.33, Theta = π / 5 [rad].

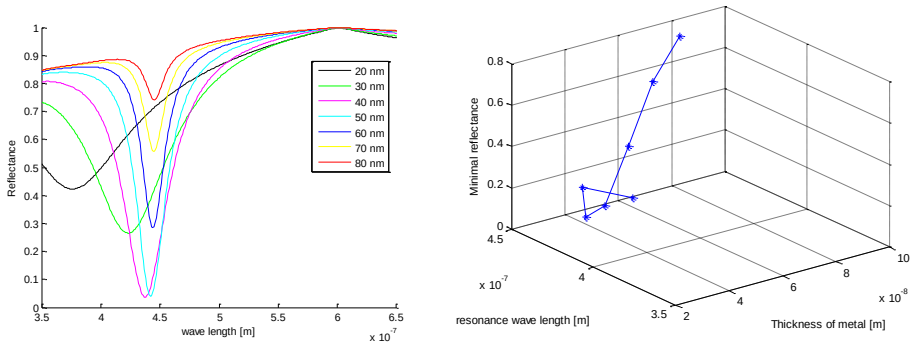

(a) *(b)*

Fig 5. a) Variation of the reflectance as a function of the wavelength and different values of dAg; b) Variation of the minimum reflectance as a function of the resonance wavelength and the metal thickness dAg: n1 = 2.7, n2 = 1.33, Theta = π / 5 [rad].

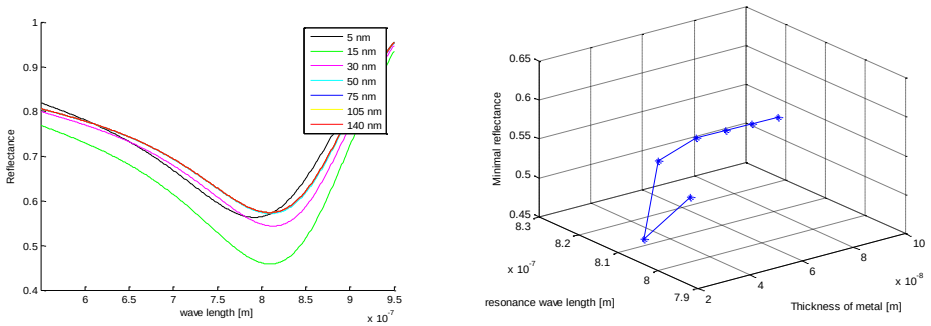

Fig 6. a) Variation of the reflectance as a function of the wavelength and different values of dAl; b) Variation of the minimum reflectance as a function of the resonance wavelength and the metal thickness dAl: n1 = 6.5, n2 = 1.33, Theta = π / 5 [rad].

To get a better response from the SPR sensor, the reflection should go towards 0% (total reflection), so in the following, the study based on Gold and Silver with 2% and 3% of minimum reflectance respectively, and we leave Aluminum by 45 % of minimum reflectance. Since it is that the SPR response of a biomedical detector structure is based on the detection of change in the SPR wavelength as a function of change in the optical properties of the biological medium studied (the refractive index) [12]. Slavik and Homola (1999) developed a SPR sensor for the operating range 1.343–1.352 of refractive index of detected analyte [19], so the SPR response based on this range of refractive index. It is assumed that the biological medium studied is positioned under the metal with a refractive index n2, The SPR response based on Gold and Silver are presented in Figs. 7 and 8, respectively.

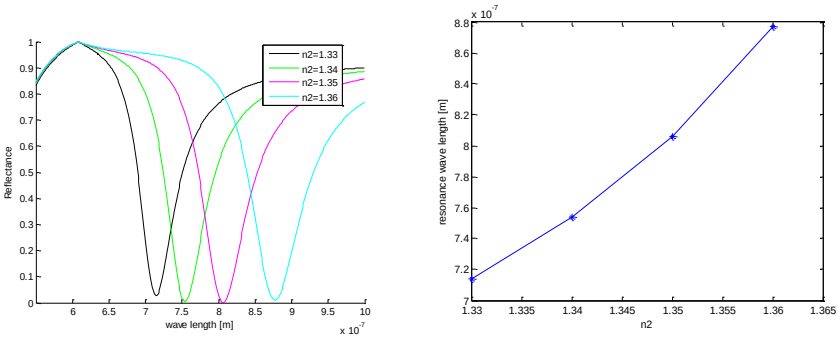

(a) *(b)*

Fig 7. a) Variation of the reflectance as a function of the wavelength and different values of n2; b) Variation of the resonance wavelength as a function of n2: n1 = 2.39, Theta = π / 5 [rad], dAu = 50 [nm] [20].

We note that the SPR effect is present in all the reflectance curves with the parametric and geometric conditions presented in the figures (Figs. 7.a and 8.a). On the other hand, the SPR response of the two metals studied is almost linear (Figs. 7.b and II.8.b) with a sensitivity of 5.43×10^{-6} [m] and 7.66×10^{-7} [m] for gold and silver respectively. So, from the results obtained, we can say that Gold is the best material for the application in the field of SPR detection.

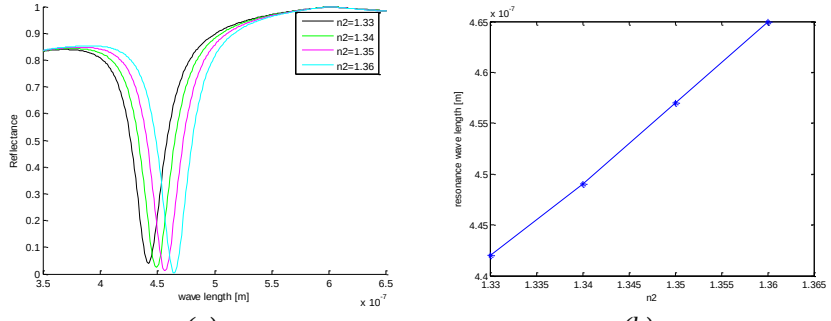

(a) *(b)*

Fig 8. a) Variation of the reflectance as a function of the wavelength and different values of n2; b) Variation of the resonance wavelength as a function of n2: n1 = 2.7, Theta = π / 5 [rad], dAg = 50 [nm] [20].

The second structure studied in five layers is presented in Figure 9. Where there are five layers with complex refractive indexes n_1, n_2, nm, n_3, and n_4.

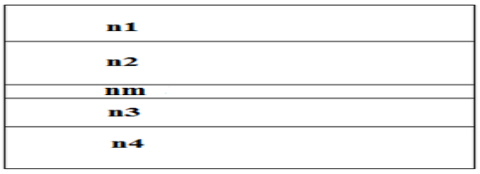

Fig 9. Structure studied in five layers.

It is assumed that the biological medium being studied is positioned under the metal with a refractive index n_4, so, the SPR response based on Gold and Silver are presented in Figs. 10 and 11 respectively. We note that the SPR effect is present in all reflectance curves with the parametric and geometrical conditions presented in the figures (Figs. 10.a, 11.a).

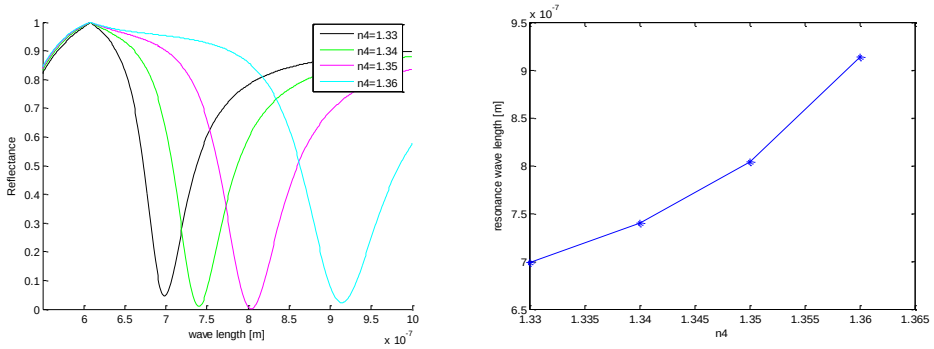

(a) *(b)*

Fig 10. a) Variation of the reflectance as a function of the wavelength and different values of n4; b) Variation of the resonance wavelength as a function of n4: n1 = 2.35, n2 = 1.77, d2 = 1 [nm], n3 = 1.2, d3 = 25 [nm], dAu = 50 [nm] [20].

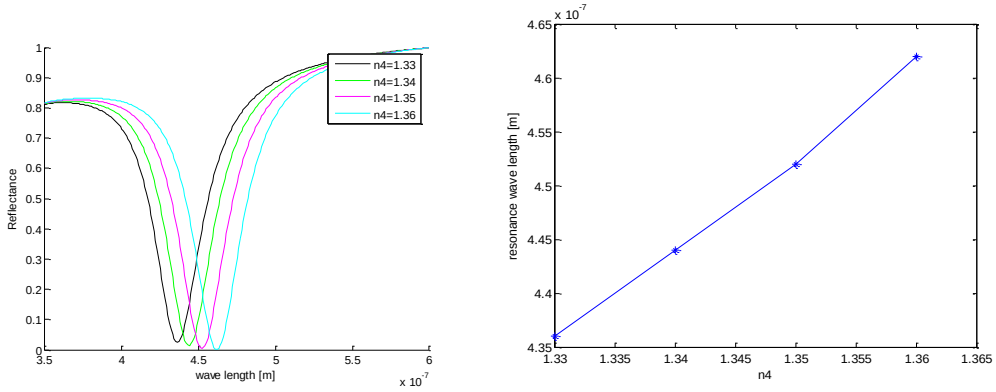

(a) *(b)*

Fig 11. a) Variation of the reflectance as a function of the wavelength and different values of n4; b) Variation of the resonance wavelength as a function of n4: n1 = 2.5, n2 = 1.77, d2 = 1 [nm], n3 = 1, d3 = 10 [nm], dAg = 50 [nm] [20].

We notice the SPR response is almost linear (Figs. 10.b, 11.b) with a sensitivity of 7.16×10^{-6} [m] for Gold and 8.66×10^{-7} [m] for Silver. From the results obtained, it is possible to increase the sensitivity of the detector SPR structure by the play on the optical parameters and the geometry of the layers constitutes the SPR structure.

4. Conclusions

In this paper, we presented the theatrical study of the response of a multilayer SPR detector structure. The work carried out focused on the part of the design of the structure and the response of the latter in the optical band visible in TM mode based on the T-Matrix semi-analytical method and the Matlab software. In the beginning, we carried out the design of the multilayer SPR structure studied, we proposed dimensions of the structure studied and adapted the optical properties of the layers with these dimensions of tell out the effect SPR exists in the response of the studied structure in reflection in wavelength of incidence, This is the first challenge. The results of the simulation that we obtained and the theoretical approach that led to it, show that the SPR effect is influenced by the type and thickness of the metal used in the structure, and the optical properties and the thicknesses of the layers that make up the structure. The response of the studied SPR structure gives us: the best thickness of the metal is around the operating range 50-15 [nm] for a better resolution of the answer, and that Gold is the best material for the application in the field of the detection SPR compared by Silver and Aluminum. From the results obtained, it is possible to increase the sensitivity of the detector SPR structure by the play on the optical parameters and the geometry of the layers constitutes the SPR structure. Finally and with the comparison between the results obtained and the SPR detector data in Handbook of Surface Plasmon Resonance [12] proves that we can practice this device in the field of biomedical detection.

R E F E R E N C E S

[1]. *Liedberg, C. Nylander and I. Lundström*, "SURFACE PLASMON RESONANCE FOR GAS DETECTION AND BIOSENSING", Sens. Actuators., **vol. 4**, 1983, pp. 299–304.

[2]. *L. Touahir, E. Galopinb, et all,* "Localized surface plasmon-enhanced fluorescence spectroscopy for highly-sensitive real-time detection of DNA hybridization", Biosensors and Bioelectronics., **vol. 25**, 2010. pp. 2579–2585.

[3]. *Z. Zhan, X. Ma, et all*, "Gold-based optical biosensor for single-mismatched DNA detection usingsalt-induced hybridization", Biosensors and Bioelectronics., **vol. 32**, 2012, pp. 127–132.

[4]. *Y. Liu, J. Kim*, "Numerical investigation of finite thickness metal-insulator-metal structure for waveguide-based surface plasmon resonance biosensing", Sensors and Actuators B: Chemical., **vol. 148**, 2010, pp. 23–28.

[5]. *Gerardo A. López-Muñoz et al,* "A label-free nanostructured plasmonic biosensor based on Blu-ray discs with integrated microfluidics for sensitive biodetection", Biosensors and Bioelectronics., **vol. 96**, 2017, pp. 260-267.

[6]. *Subash C.B. Gopinath*, "Biosensing applications of surface plasmon resonance-based Biacore technology", Sensors and Actuators B., **vol. 150**, 2010, pp. 722–733.
[7]. *N. G. Khlebtsov, L. A. Dykman*, "Optical properties and biomedical applications of plasmonic nanoparticles", Journal of Quantitative Spectroscopy & Radiative Transfer., **vol. 111**, 2010, pp. 1–35.
[8]. *C. Lin, K. Chen, et all*, "Bio-plasmonics: Nano/microstructure of surface plasmon resonance devices for biomedicine", Optical and Quantum Electronics., **vol. 37**, 2005, pp. 1423–1437.
[9]. *T. Vo-Dinh, F. Yan, and D. L. Stokes*, "Plasmonics-Based Nanostructures for Surface-Enhanced Raman Scattering Bioanalysis", Methods in Molecular Biology., **vol. 300**, vol N°. 12, 2005, pp. 255–282.
[10]. *T. Riedel, F. Surman et al*, "Hepatitis B plasmonic biosensor for the analysis of clinical serum samples", Biosensors and Bioelectronics., **vol. 85**, 2016, pp. 272–279.
[11]. A. *Elmholdt Christensen, C. Uhrenfeldt, et all*, "Interaction between Au nanoparticles and Er3+ ions in a TiO2 matrix: Up-conversion of infrared light", Energy Procedia., **vol. 10**, 2011, pp.111–116.
[12]. *Di Qu, Fang Liu, Xujie Pan, et all*, "PLASMONIC CORE-SHELL NANOPARTICLE ENHANCED OPTICAL ABSORPTION IN THIN FILM ORGANIC SOLAR CELLS", Photovoltaic Specialists Conference (PVSC), 37th IEEE, 2011, pp. 924–928.
[13]. Richard B. M. Schasfoort, "Handbook of Surface Plasmon Resonance", 2nd Edition, Royal Society of Chemistry, 2017, p. 544.
[14]. *D. Courjon, C. Bainier*, "Le champ proche optique théorie et applications", Livre, Springer Science & Business Media, 2001.
[15] *Thomas E., Furtak Miles V Klein*, "Optics", wely, 2eme edition, 1986, p. 676.
[16]. A. C., Polycarpou, "Introduction to the Finite Element Method in Electromagnetics", (book), **vol.01**, 2006, Printed in the United States of America.
[17]. *J. Singh*, "Optical Properties of Condensed Matter and Applications", Livre, edition Wiley & Sons, 2006, pp. 440.
[18]. *A. Vial and T. Laroche*, "Description of dispersion properties of metals by means of the critical points model and application to the study of resonant structures using the FDTD method", J. Phys. D : Appl. Phys., **vol. 40**, 2007, pp. 7152–7158.
[19]. *R. Slavik, J.Homola, and J. Ctyriky*, "Single-mode optical fiber surface Plasmon resonance sensor", Sensors and Actuators B., **vol. 54**, 1999, pp.74-79.
[20] *Saouli Abdelali, Saouli Chouaib*, "Simulation of spectral response of SPR multilayers nanostructures detector intended for biomedical application", Materials Today: Proceedings., **vol. 31**, 2020, pp.S24-S27.